



# ANTHROPOGENIC CONTRIBUTIONS TO THE 2018 EXTREME FLOODING OVER THE UPPER YELLOW RIVER BASIN IN CHINA

PENG JI, XING YUAN, YANG JIAO, CHUNQING WANG, SHUAI HAN, AND CHUNXIANG SHI

Anthropogenic climate change, reservoir operation, and land cover change have decreased the risk of 2018 extreme summer flooding by 34%, 45%, and 11% respectively.

The Upper Yellow River basin (UYRB), located over northwestern China and featuring a semiarid climate, experienced extreme flooding during the summer and autumn of 2018, with June–September rainfall ranked the highest since 1961 (CMA 2019). The extreme flooding affected about 1.4 million people and led to 30 deaths and disappearances. Many reservoirs exceeded their historical water levels to mitigate the floods, but the monthly mean streamflow during rainy season (June–September) over the UYRB still exceeded its historical value since 1987 when a large reservoir started to operate.

In the Anthropocene, water resources management such as reservoir operation changes streamflow characteristics significantly (Yuan et al. 2017).

For instance, Yuan et al. (2018a) found that water resources management contributes up to 27% of the long-term changes in streamflow and its extremes over the middle reaches of the Yellow River. However, contributions from different anthropogenic factors (e.g., anthropogenic climate change, local human interventions) to the occurrence of a single extreme hydrological event (e.g., 2018 extreme flooding) remain unclear, especially for regions where both land and water are managed intensively (e.g., the UYRB).

Here we investigate the anthropogenic contributions to the 2018 extreme summer flooding over the UYRB in the context of anthropogenic climate change, regional water resources management, and land cover change, by using observed and naturalized streamflow data together with a high-resolution land surface model driven by different climate forcings.

**AFFILIATIONS:** JI—Key Laboratory of Regional Climate-Environment for Temperate East Asia, Institute of Atmospheric Physics, Chinese Academy of Sciences, and College of Earth and Planetary Sciences, University of Chinese Academy of Sciences, Beijing, China; YUAN—Key Laboratory of Regional Climate-Environment for Temperate East Asia, Institute of Atmospheric Physics, Chinese Academy of Sciences, Beijing, and School of Hydrology and Water Resources, Nanjing University of Information Science and Technology, Nanjing, China; JIAO—School of Hydrology and Water Resources, Nanjing University of Information Science and Technology, Nanjing, China; WANG—Hydrology Bureau of Yellow River Conservancy Commission, Zhengzhou, China; HAN AND SHI—National Meteorological Information Center, China Meteorological Administration, Beijing, China

**CORRESPONDING AUTHOR:** Xing Yuan, xyuan@nuist.edu.cn

DOI:10.1175/BAMS-D-19-0105.1

A supplement to this article is available online (10.1175/BAMS-D-19-0105.2)

© 2020 American Meteorological Society  
For information regarding reuse of this content and general copyright information, consult the [AMS Copyright Policy](#).

**DATA AND METHODS.** *Streamflow data.* Daily streamflow observation during 1987–2018 at Lanzhou station, a large hydrological station over the UYRB (orange pentagram in Fig. 1a), was provided by the Yellow River Conservancy Commission (YRCC) to analyze the extreme flooding. Monthly naturalized streamflow during 1987–2010 was also provided by YRCC, which was estimated by adding human consumed water (including agricultural, industrial, and civil uses) back to the observation (Fu et al. 2004; Yuan et al. 2017). The naturalized streamflow was used to evaluate performance of the land surface model.

*Meteorological observation data.* Monthly geopotential height and vertical integrated water vapor flux during 1979–2018 from the ERA-Interim reanalysis (Dee et al. 2011) were used to show circulation anomalies during the flooding seasons. The meteorological forcings for high-resolution land surface

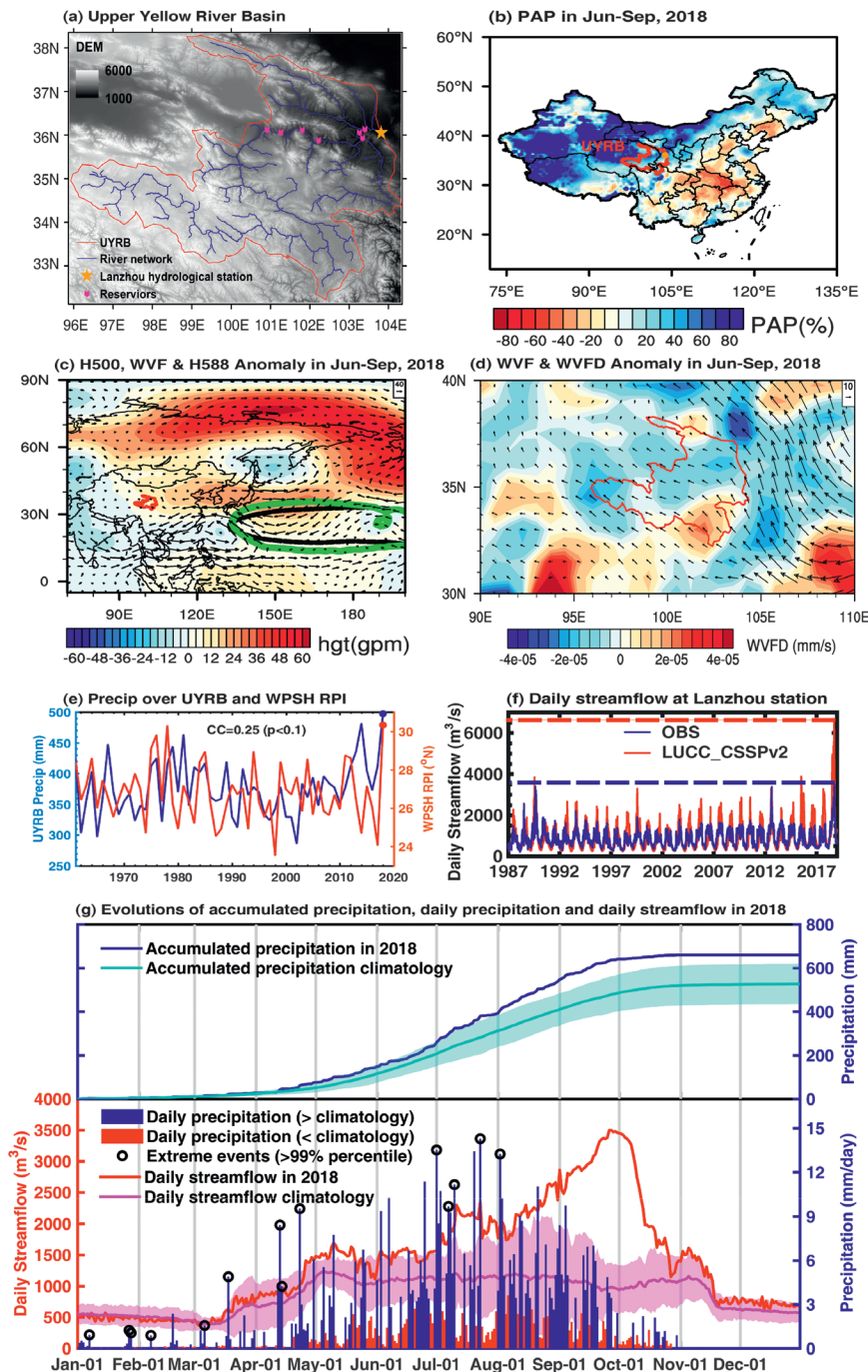


**FIG. 1.** (a) The Upper Yellow River basin (UYRB). (b) Percentage anomaly of precipitation (PAP) during June–September of 2018 compared with the 1961–2018 climatology. (c) June–September mean geopotential height anomaly at 500 hPa (shading), and integrated water vapor flux (WVF) anomaly (vectors) in 2018. Green and black lines show the 5,880-gpm contours for 2018 and 1979–2018 climatology, respectively. (d) Divergence of WVF over UYRB. (e) Time series of June–September mean precipitation averaged over the UYRB, and western Pacific subtropical high ridge position index. (f) Observed and LUC\_CSSPv2-simulated daily streamflow. (g) Observed 2018 daily precipitation and streamflow as compared with their climatology. Shaded areas are 95% confidence intervals. Red and blue bars represent daily precipitation cases that are smaller and larger than its climatology respectively.

modeling were generated as follows: 1) the  $0.5^\circ \times 0.5^\circ$  CRUNCEP dataset (Viovy 2011) during 1951–2016 was first regridded to 10-km resolution; 2) daily precipitation and temperature data were replaced by gridded observational dataset during 1951–2018, which was interpolated from more than 2,470 China Meteorological Administration (CMA) stations in China (Wang et al. 2016; Wu et al. 2017); 3) other forcings including daily specific humidity, surface shortwave radiation, wind speed, and surface pressure were extended to 2018 by using the  $0.0625^\circ \times 0.0625^\circ$  CMA Land Data Assimilation System dataset (CLDAS; Meng et al. 2017), where the CLDAS dataset was adjusted to CRUNCEP climatology during the overlap period of 2008–16 through quantile-mapping; and 4) the  $0.1^\circ$  China Meteorological Forcing Dataset during 1979–2014, which performs well in shortwave radiation (He and Yang 2011), was used to correct the systematic bias of CRUNCEP radiation at monthly time scale.

*CMIP5 model data.* Daily precipitation and temperature from 13 models from phase 5 of the Coupled Model Inter-comparison Project (CMIP5) (see Table ES1 in the online supplemental material for the model list) during 1951–2005 under both historical (ALL) and natural (NAT) scenarios were also interpolated to 10-km resolution. The 10-km resolution is chosen to reasonably represent land surface information such as

topography and soil texture, which are important for streamflow modeling. All models well capture the temperature and precipitation distribution, with spatial correlation coefficients during rainy season ranging from 0.56 to 0.93. However, the spatial mean biases of annual temperature and precipitation range from  $-0.7^{\circ}$  to  $-3.7^{\circ}\text{C}$  and 114 to 720 mm respectively (Figs. ES1a,b), which may cause large biases in streamflow simulations. Thus we reduced the biases by applying a cumulative distribution function (CDF) matching method (Wood et al. 2002) at monthly time scale (see the supplemental material for detailed information).

**Experimental design.** The land surface model, Con-junctive Surface-Subsurface Process model version 2 (CSSPv2; Yuan et al. 2018b), which well captures hydrological variations over the UYRB (Yuan et al. 2018b), was used for streamflow simulation in this study. Monthly Leaf Area Index (LAI) values during 1982–2018 estimated from the Global Inventory Modeling and Mapping Studies (GIMMS) and MODIS Normalized Difference Vegetation Index (NDVI; Yuan et al. 2018b) were used to represent land cover change.

Differences between observed and naturalized streamflow are attributed to human water intervention (mainly from reservoir operation over the UYRB). Due to the lack of data, the CSSPv2 model was first driven by modified CRUNCEP data with interannual LAI variations (LUCC\_CSSPv2) to provide daily naturalized streamflow. Evaluation results (see the online supplement for detailed information) show that LUCC\_CSSPv2 well simulates naturalized streamflow with high Nash–Sutcliffe efficiency (up to 0.87) and low relative bias ( $-3\%$  to  $-2\%$ ). Second, CSSPv2 was driven by the modified CRUNCEP dataset with LAI fixed in 1982 (FIXED\_CSSPv2). The difference between LUCC\_CSSPv2 and FIXED\_CSSPv2 is the impact of land cover change. Third, the CSSPv2 model was forced by bias-corrected CMIP5 model outputs under ALL (ALL/FIXED\_CSSPv2) and NAT (NAT/FIXED\_CSSPv2) scenarios without land cover change, to distinguish the anthropogenic climate change impacts. Although ALL simulations implicitly include land use/cover change (LUCC) information to some extent, most of them cannot capture the interannual variations of land cover at regional scale due to the deficiencies in the vegetation dynamics models (Bao et al. 2014). Therefore, here we ignore the LUCC effect in these CMIP-driven experiments.

**Definition of extreme streamflow and attribution methods.** In this study, the annual maximum daily stream-

flow is defined as high flow, whose distribution was estimated by the generalized extreme value (GEV) distribution. The probability of high flow exceeding a value of  $3,500\text{ m}^3\text{ s}^{-1}$  is defined as the probability of extreme flooding like that of 2018. The risk ratio (Fischer and Knutti 2015) is then calculated as  $RR_i = P_i/P_{\text{NAT}}$ , where  $i$  represents different scenarios and  $P_{\text{NAT}}$  is the probability of extreme flooding without any anthropogenic effects. Due to the errors in CMIP5 simulations, the distribution of ALL/FIXED\_CSSPv2 is not necessarily identical to FIXED\_CSSPv2. Thus  $P_{\text{NAT}}$  is not equal to  $P_{\text{NAT}/\text{FIXED\_CSSPv2}}$ . However, assuming that the ALL/FIXED\_CSSPv2 and NAT/FIXED\_CSSPv2 can provide a reliable estimation of anthropogenic climate change effect through their intercomparison,  $P_{\text{NAT}}$  can be estimated through the assumption of

$$\frac{P_{\text{ALL}/\text{FIXED\_CSSPv2}}}{P_{\text{NAT}/\text{FIXED\_CSSPv2}}} = \frac{P_{\text{FIXED\_CSSPv2}}}{P_{\text{NAT}}}$$

How much impact an anthropogenic factor would have on the likelihood of extreme flooding event can be directly calculated by comparing risk ratios in different experiments (see the supplemental material for detailed information). We repeated the above calculation of risk ratio and return period by doing bootstrapping 10,000 times. During each bootstrap, high flow data under different scenarios were resampled with replacement to get a set of new data with the same length as the original (Paciorek et al. 2018). Median value was used as mean value to avoid outliers (e.g., infinite), while 2.5% and 97.5% percentiles were used to estimate uncertainties at 95% confidence level.

**RESULTS.** Large positive anomalies of June–September precipitation over northwestern China in 2018 (Fig. 1b) are related to the anomalous position of the western Pacific subtropical high (WPSH). Represented by geopotential height contour at 5,880 gpm, the WPSH in 2018 (green line in Fig. 1c) shifts to the north compared with its climatology position during 1979–2018 (black line in Fig. 1c). The northernmost WPSH, revealed by WPSH Ridge Position Index (RPI) (Fig. 1e), correlates well with UYRB rainfall because the northward WPSH brings sufficient water vapor from northwestern Pacific and South China Sea to the northwestern China through the southeastern wind anomaly, causing a convergence of water vapor in UYRB (Fig. 1d) and thus providing favorable conditions for precipitation. Under this background,

precipitation is larger than its climatology for most days during June–September in 2018, with five days showing extreme rainfall events (>99% percentile) (Fig. 1g). Land surface becomes saturated due to this seasonal-scale positive precipitation anomaly, which then reduces infiltration capacity and increases both surface and subsurface runoff. As a result, daily streamflow starts to increase in June, significantly exceeds its climatology during July–September, and reaches its maximum when the accumulated precipitation reaches its maximum in late September. Naturalized streamflow (LUCC\_CSSPv2) shows that the high flow could be  $6,622 \text{ m}^3 \text{ s}^{-1}$ , with a return period of 242 yr (95% CI: >82 yr) (Fig. 1f). However, due to reservoir operation over the UYRB, the observed value is only  $3,500 \text{ m}^3 \text{ s}^{-1}$ , with a return period of 50 yr (95% CI: 27–130 yr).

Figures 2a and 2b show probability distribution functions (PDFs) of high flow with or without LUCC or reservoir operation effects, together with their 95% confidence intervals. The significant leftward

shifting of the PDFs suggests that both land cover change and reservoir regulation decrease extreme high flow occurrence. As compared with natural climate change conditions, anthropogenic climate change also decreases probability of extreme high flow (Fig. 2c).

Table 1 shows return period and risk ratio of the 2018 extreme flooding under different scenarios. Without any anthropogenic influence (NAT scenario), this extreme event occurs frequently with a 5-yr (95% CI: 3–10 yr) return period. When anthropogenic climate change, land cover change, and reservoir operation are gradually considered, the risk ratio decreases to 0.66 (95% CI: 0.56–0.82), 0.55 (95% CI: 0.44–0.68), and 0.1 (95% CI: 0.04–0.17) respectively. The risk ratio decreases significantly by 0.34 (95% CI: 0.18–0.44) from NAT to FIXED\_CSSPv2, by 0.11 (95% CI: 0.08–0.21) from FIXED\_CSSPv2 to LUCC\_CSSPv2, and by 0.45 (95% CI: 0.34–0.57) from LUCC\_CSSPv2 to YRCC observed streamflow scenarios.

Different from reservoir operation, which reduces

the probability of flooding by controlling the surface runoff, increased vegetation cover ( $p < 0.01$ ) over the UYRB (Fig. ES2a) caused by conservation programs (Cuo et al. 2013) increases evapotranspiration during June–September (Fig. ES2b) and reduces soil moisture and thus subsurface runoff (Fig. ES2c). Anthropogenic climate change reduces surface runoff (Fig. ES2e) by significantly reducing the seasonal precipitation (Fig. 2d) instead of the extreme precipitation (Fig. 2e). The negative effect of anthropogenic climate change on seasonal precipitation occurs because the descending branch of Hadley circulation over the edges ( $\sim 30^\circ$  to  $\sim 40^\circ \text{N}$ ) enhances in a warming climate (Su et al. 2014), which inhibits precipitation generation. Moreover, anthropogenic climate change increases evapotranspiration (Fig. ES2d), thus reducing soil moisture

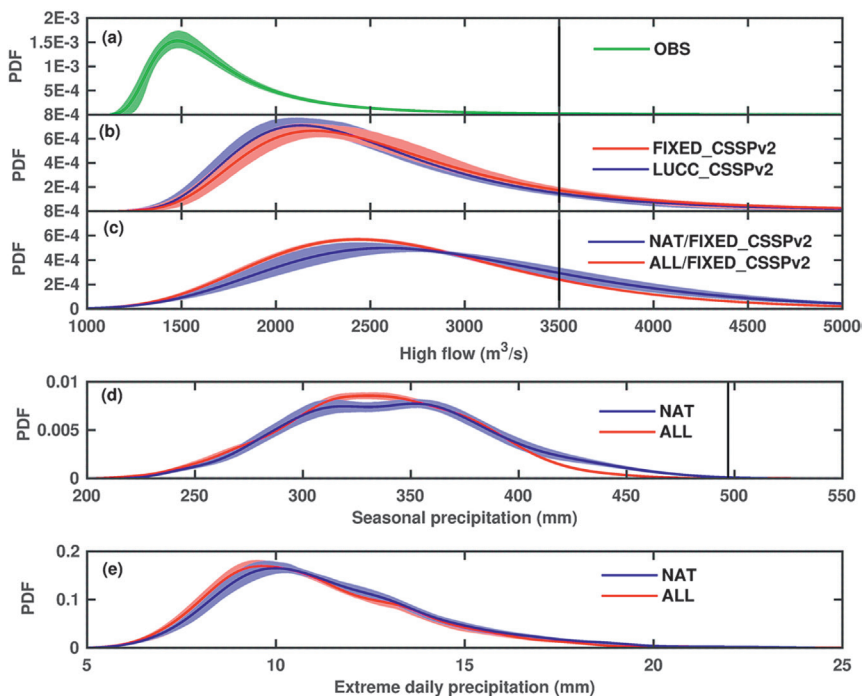


**FIG. 2.** (a) Probability distribution functions (PDFs) of observed high flow (green). (b) PDFs of CSSPv2-simulated high flows with (LUCC\_CSSPv2) or without (FIXED\_CSSPv2) land cover changes. (c) PDFs of simulated high flow forced by CMIP5 ALL (ALL/FIXED\_CSSPv2) and NAT (NAT/FIXED\_CSSPv2) climate output (see Methods section for details). Black lines in (a)–(c) represent the high flow threshold value of 2018. (d) PDFs of June–September mean precipitation under ALL and NAT scenarios, with the black line showing extreme rainfall in 2018. (e) PDFs of extreme daily precipitation (>99% percentile) under ALL and NAT scenarios. All the shading areas represent 95% confidence intervals.

as well as subsurface runoff (Fig. ES2e).

## CONCLUSIONS AND DISCUSSION.

Anthropogenic contributions to the 2018 extreme flooding event were analyzed by considering large-scale anthropogenic climate change and local human interventions.

The probability for the occurrence of the event decreases by 90% due to those anthropogenic factors, with anthropogenic climate change, land cover change, and reservoir regulation contributing by 34%, 11%, and 45% respectively.

As risk ratios are all relative to the NAT condition in this study, this makes it easy to compare different risk ratio under different scenarios. For example, by comparing the risk ratio of YRCC observed streamflow and LUCC\_CSSPv2, reservoir operation decreases the risk of extreme flooding in the LUCC\_CSSPv2 scenario by 82%. However, as the probability of extreme flooding in LUCC\_CSSPv2 is only 55% of that in NAT scenario, the value will be 45% ( $0.82 \times 0.55$ ) again when we use the extreme flooding probability in NAT scenario as a reference.

The attribution results proposed in this study have uncertainties. For example, the land cover change cannot be interpreted solely as local human intervention as other factors including climate change and CO<sub>2</sub> fertilization also have contributions. However, as climate models have large uncertainty in simulating vegetation dynamics (Bao et al. 2014), it is still a great challenge to attribute land cover changes under different scenarios. Biases in land surface model may cause uncertainties in human water intervention attributions. However, considering the low bias of CSSPv2 in reproducing natural conditions (−3% to −2%), the model uncertainty should be limited and it does not influence the results significantly.

Our results highlight the importance of local-scale human influences in hydrological attributions, as anthropogenic contributions may be underestimated by 60% (56% relative to 90%) without considering them. More efforts should be made to incorporate local-scale human activities in current global climate models (GCMs), as most GCMs do not have representation of water management or vegetation dynamics due to coarse resolution, imperfect parameterizations, etc. (Fisher et al. 2018; Trenberth and Asrar 2014).

**TABLE 1. Summary of return period of the 2018 extreme flooding under different scenarios together with the risk ratio (RR). The 95% confidence intervals are shown in parentheses.**

Different scenarios	Return period (95% CI)	RR (95% CI)
NAT	5 yr (3–10 yr)	1
FIXED_CSSPv2	7 yr (5–14 yr)	0.66 (0.56–0.82)
LUCC_CSSPv2	9 yr (7–19 yr)	0.55 (0.44–0.67)
YRCC observed streamflow	50 yr (27–130 yr)	0.1 (0.04–0.17)

**ACKNOWLEDGMENTS.** We acknowledge the World Climate Research Programme’s Working Group on Coupled Modeling, which is responsible for CMIP. This work was supported by National Key R&D Program of China (2018YFA0606002) and National Natural Science Foundation of China (41875105, 91437220).

## REFERENCES

- Bao, Y., and Coauthors, 2014: Evaluation of CMIP5 Earth system models in reproducing leaf area index and vegetation cover over the Tibetan Plateau. *J. Meteor. Res.*, **28**, 1041–1060, <https://doi.org/10.1007/s13351-014-4023-5>.
- CMA, 2019: China Climate Bulletin 2018. China Meteorological Administration, 56 pp, [http://www.cma.gov.cn/root7/auto13139/201903/t20190319\\_517664.html](http://www.cma.gov.cn/root7/auto13139/201903/t20190319_517664.html).
- Cuo, L., Y. Zhang, Y. Gao, Z. Hao, and L. Cairang, 2013: The impacts of climate change and land cover/use transition on the hydrology in the upper Yellow River basin, China. *J. Hydrol.*, **502**, 37–52, <https://doi.org/10.1016/j.jhydrol.2013.08.003>.
- Dee, D. P., and Coauthors, 2011: The ERA-Interim reanalysis: Configuration and performance of the data assimilation system. *Quart. J. Roy. Meteor. Soc.*, **137**, 553–597, <https://doi.org/10.1002/qj.828>.
- Fischer, E. M., and R. Knutti, 2015: Anthropogenic contribution to global occurrence of heavy-precipitation and high-temperature extremes. *Nat. Climate Change*, **5**, 560–564, <https://doi.org/10.1038/nclimate2617>.
- Fisher, R. A., and Coauthors, 2018: Vegetation demographics in Earth system models: A review of progress and priorities. *Global Change Biol.*, **24**, 35–54, <https://doi.org/10.1111/gcb.13910>.
- Fu, G., S. Chen, C. Liu, and D. Shepard, 2004: Hydroclimatic trends of the Yellow River Basin for the last 50 years. *Climatic Change*, **65**, 149–178, <https://doi.org/10.1023/B:CLIM.0000037491.95395.bb>.
- He, J., and K. Yang, 2011: China meteorological forcing dataset. Cold and Arid Regions Science Data

- Center, accessed March 2019, Lanzhou. <https://doi.org/10.3972/westdc.002.2014.db>.
- Meng, X., H. Wang, Y. Wu, A. Long, J. Wang, C. Shi, and X. Ji, 2017: Investigating spatiotemporal changes of the land-surface processes in Xinjiang using high-resolution CLM3.5 and CLDAS: Soil temperature. *Sci. Rep.*, **7**, 13286, <https://doi.org/10.1038/s41598-017-10665-8>.
- Paciorek, C. J., D. A. Stone, and M. F. Wehner, 2018: Quantifying statistical uncertainty in the attribution of human influence on severe weather. *Wea. Climate Extremes*, **20**, 69–80, <https://doi.org/10.1016/j.wace.2018.01.002>.
- Pall, P., T. Ainu, D. A. Stone, P. A. Stott, T. Nozawa, A. G. J. Hilberts, D. Lohmann, and M. R. Allen, 2011: Anthropogenic greenhouse gas contribution to flood risk in England and Wales in autumn 2000. *Nature*, **470**, 382–385, <https://doi.org/10.1038/nature09762>.
- Su, H., J. H. Jiang, C. X. Zhai, T. J. Shen, J. D. Neelin, G. L. Stephens, and Y. L. Yung, 2014: Weakening and strengthening structures in the Hadley circulation change under global warming and implications for cloud response and climate sensitivity. *J. Geophys. Res. Atmos.*, **119**, 5787–5805, <https://doi.org/10.1002/2014JD021642>.
- Trenberth, K. E., and G. R. Asrar, 2014: Challenges and opportunities in water cycle research: WCRP contributions. *Surv. Geophys.*, **35**, 515–532, <https://doi.org/10.1007/s10712-012-9214-y>.
- Viovy, N. 2011: CRUNCEP dataset [CRUNCEP is for Climatic Research Unit and National Centers for Environmental Prediction]. Accessed March 2019; description available at <http://dods.extra.cea.fr/data/p529viov/cruncep/readme.htm>; data available at [http://dods.extra.cea.fr/store/p529viov/cruncep/V4\\_1901\\_2011/](http://dods.extra.cea.fr/store/p529viov/cruncep/V4_1901_2011/).
- Wang, L., X. Yuan, Z. Xie, P. Wu, and Y. Li, 2016: Increasing flash droughts over China during the recent global warming hiatus. *Sci. Rep.*, **6**, 30571, <https://doi.org/10.1038/srep30571>.
- Wood, A. W., E. P. Maurer, A. Kumar, and D. P. Lettenmaier, 2002: Long-range experimental hydrologic forecasting for the eastern United States. *J. Geophys. Res.*, **107**, 4429, <https://doi.org/10.1029/2001JD000659>.
- Wu, J., X. Gao, F. Giorgi, and D. Chen, 2017: Changes of effective temperature and cold/hot days in late decades over China based on a high resolution gridded observation dataset. *Int. J. Climatol.*, **37**, 788–800, <https://doi.org/10.1002/joc.5038>.
- Yuan, X., M. Zhang, L. Wang, and T. Zhou, 2017: Understanding and seasonal forecasting of hydrological drought in the Anthropocene. *Hydrol. Earth Syst. Sci.*, **21**, 5477–5492, <https://doi.org/10.5194/hess-21-5477-2017>.
- , Y. Jiao, D. Yang, and H. Lei, 2018a: Reconciling the attribution of changes in streamflow extremes from a hydroclimate perspective. *Water Resour. Res.*, **54**, 3886–3895, <https://doi.org/10.1029/2018WR022714>.
- , P. Ji, L. Wang, X. Z. Liang, K. Yang, A. Ye, Z. B. Su, and J. Wen, 2018b: High-resolution land surface modeling of hydrological changes over the Sanjiangyuan region in the eastern Tibetan Plateau: 1. Model development and evaluation. *J. Adv. Model. Earth Syst.*, **10**, 2806–2828, <https://doi.org/10.1029/2018MS001412>.